Frontiers in Bioscience Landmark

Front. Biosci. (Landmark Ed) **2025**; 30(5): 36971
https://doi.org/10.31083/FBL36971

Original Research

METTL3-Driven m6A Modification of *Cpt1a* Gene in High Fat Diet Related Liver Cancer Tumor Macrophages Facilitates Type II Macrophage Differentiation

Limei Zhu[1,*,†], Xuelian Li[1,†], Wenting Wang[1]

[1]Department of Clinical Laboratory, The First People's Hospital of Lianyungang, 222001 Lianyungang, Jiangsu, China
*Correspondence: zhulimei0222@163.com (Limei Zhu)
[†]These authors contributed equally.

Academic Editor: Amancio Carnero Moya
Submitted: 9 January 2025 Revised: 31 March 2025 Accepted: 11 April 2025 Published: 26 May 2025

Abstract

Objective: Obesity induces chronic inflammation and hormonal imbalances that contribute to tumor growth. This study explores the less understood dynamics of tumor-related macrophages under a high-fat diet and its consequent impact on tumor growth, with a focus on elucidating the role of high-fat diets on macrophage behavior in liver cancer. **Methods**: We established a mouse obesity model using a high-fat diet, combined with a liver cancer implantation approach. Tumor-infiltrating macrophages were isolated for analysis. We investigated the specific effects of a high-fat diet on macrophages through transcriptomic and metabolomic studies and further explored the influence of N6-methyladenosine (m6A) RNA modification on macrophage differentiation using *in vitro* and *in vivo* models. **Results**: Our findings reveal that a high-fat diet significantly accelerates *in-situ* liver cancer growth and fosters type II differentiation of tumor-associated macrophages. RNA sequencing indicated upregulation of *Cpt1a* and *Mettl3* genes, which are crucial for m6A modification in macrophages. Using human and mouse macrophage cell lines with either elevated *Mettl3* expression or *Cpt1a* gene knockout, we demonstrated that methyltransferase-like 3 (METTL3) enhances fatty acid metabolism in macrophages, a process reversible by *Cpt1a* gene knockout. These effects were corroborated *in vivo*. Further, macrophages infused with high *Mettl3* expression, when combined with an *in-situ* implantation model and adoptive cell therapy, markedly promoted liver cancer growth and increased type II macrophage differentiation ($p < 0.001$). Knockout of the *Cpt1a* gene counteracted the METTL3 effect compared to the control group ($p > 0.05$). METTL3 and m6A RNA Immunoprecipitation (RIP) assays confirmed that METTL3 stabilizes *Cpt1a* mRNA. Additionally, multispectral staining of clinical specimens revealed a positive correlation between METTL3 protein levels in liver cancer tumor-associated macrophages and M2 macrophage prevalence, inversely correlating with M1 macrophages ($p < 0.01$). High *Mettl3* expression in macrophages was associated with poor prognosis in liver cancer patients, correlating significantly with tumor size and tumor node metastasis (TNM) classification stage. **Conclusion**: Our research identifies that a high-fat diet elevates METTL3-driven m6A modification of carnitine palmitoyltransferase 1A (CPT1A) in tumor macrophages, fostering type II macrophage differentiation, and exacerbating liver cancer growth and immune evasion.

Keywords: high-fat diet; liver cancer; macrophage; m6A modification

1. Introduction

The global escalation of obesity presents a significant public health challenge, with the World Health Organization reporting that around 13% of the global adult population is now classified as obese, a figure that has been climbing sharply for decades. This issue transcends economic boundaries, affecting both affluent and developing nations, where rates of obesity are climbing in the wake of urbanization and the adoption of Western lifestyles [1,2]. The implications of obesity are profound, with a heightened risk of chronic conditions such as type 2 diabetes, cardiovascular diseases, certain cancers, and musculoskeletal disorders [3–5]. Furthermore, obesity often leads to diminished life expectancy and deteriorated quality of life. A common comorbidity of obesity is hyperlipidemia, which has been identified as a critical mediator in the relationship between obesity and cancer development. The high levels of lipids in the bloodstream, characteristic of hyperlipidemia, not only exacerbate the risk of metabolic and cardiovascular conditions but also provide a conducive environment for cancerous cells to initiate and progress, thus cementing the intricate link between obesity, lipid imbalances, and oncogenesis [6–8].

Obesity and hyperlipidemia are intricately linked to tumorigenesis through a web of biological pathways. Obesity itself initiates a chronic low-grade inflammatory state, with cytokines and chemokines released in this milieu fostering tumor growth [9]. It also perturbs hormonal balance, with insulin resistance and hyperinsulinemia known to be pro-carcinogenic for certain cancers. Additionally, obesity-induced alterations in sex hormone levels have been implicated in increasing the risk of breast and endometrial cancers [10]. Hyperlipidemia, particularly elevated serum cholesterol, is independently associated with tumorigene-

sis, given cholesterol's critical role in cell membrane integrity and signaling pathways; disruptions in these processes can precipitate cellular proliferation and cancer [9]. Moreover, cancer cells may exploit circulating fatty acids as a fuel source, thereby facilitating their proliferation and metastasis. Often occurring concurrently, obesity and hyperlipidemia might amplify the risk of cancer through their combined metabolic effects. High-fat diets, a common cause of both conditions, contribute to this risk by potentiating chronic inflammation, oxidative stress, and hormonal imbalances [11]. This suggests that both conditions could not only independently drive tumor development but might also act synergistically, underscoring the need for dietary and lifestyle interventions in cancer prevention strategies [12].

In our research, we induced obesity in mice through a high-fat diet regimen. Subsequent omics analyses revealed that this diet precipitates alterations in the N6-methyladenosine (m6A) modification of genes involved in lipid metabolism within macrophages associated with hepatic tumors. Further clinical investigations have corroborated that changes mediated by methyltransferase-like 3 (METTL3) in this context are intimately linked with the prognosis of liver cancer patients.

2. Materials and Methods

2.1 Clinical Specimens and Cell Lines

Paraffin-embedded human liver cancer specimens were obtained from 79 patients diagnosed between 2013 and 2015, with written informed consent obtained from all participants. This study was in accordance with the Declaration of Helsinki and approved by the Ethics in Research Committee of People's Hospital of Lianyungang, China. The THP-1 and Raw246.7 cell lines were procured from Procell Life Science & Technology Co., Ltd. (Wuhan, China). Cellular samples were incubated in an RPMI 1640 solution from Invitrogen, based in Carlsbad, California, supplemented with 10% FBS (Cat. A5256701, Invitrogen, Carlsbad, CA, USA), 100 micrograms per milliliter of streptomycin, and penicillin G at a concentration of 100 units per milliliter. Both THP-1 and Raw246.7 cell lines have undergone mycoplasma infection testing and STR validation. Cells were cultured at a constant temperature of 37 degrees Celsius within an environment containing 5% carbon dioxide. Each treatment group of cell lines has 6 replicates to render sufficient statistical power, and every experiment was performed in triplicate.

2.2 Cell Transfection

Lentiviral vectors for *Mettl3* over-expression (METTL3 OE) and *Cpt1a* knockdown (CPT1A shRNA) were obtained from GeneChem (Shanghai, China), and an empty vector was used as the negative control (NC), as specified in Table 1. Each cell line has three treatment groups: Control, METTL3 OE (Group A), and METTL3 OE + CPT1A shRNA (Group B). The Control group was transfected with empty lentiviral vectors, Group A was transfected with METTL3 OE lentiviral vectors, and Group B was transfected with METTL3 OE and CPT1A shRNA lentiviral vectors. Stable transduced cells were selected using puromycin (Cat.No.: ST551-10mg, Beyotime, Shanghai, China). To reduce batch-to-batch variation, each comparison involved pairs of samples from the same batch. All transfections were performed according to the manufacturer's instructions.

2.3 Reverse Transcription Quantitative PCR (RT-qPCR)

RNA was entirely extracted from the cells using the TRIzol reagent (Invitrogen, Carlsbad, CA, USA, Cat. No. 15596026) following the manufacturer's instructions. Subsequently, cDNA synthesis was performed with the PrimeScript RT Master Mix Kit (TaKaRa, Dalian, China, Cat. No. RR036A). Real-time PCR analysis was conducted using SYBR Premix Ex Taq (Tli RNaseH Plus) (TaKaRa, Dalian, China, Cat. No. RR420A). Gene expression levels were normalized to GAPDH, which served as the reference gene. The primers used for amplification are detailed in Table 1. After amplifying cDNA, the quantification is typically done using the $\Delta\Delta$Ct method. We first determined the threshold cycle (Ct) values for both the target and reference genes, calculated the difference (ΔCt) between them, and then compared the ΔCt values of experimental samples to a control ($\Delta\Delta$Ct). The relative expression is expressed as $2^{-\Delta\Delta Ct}$.

2.4 In Vitro Macrophage Stimulation

The THP-1 human monocyte cell line was cultivated in RPMI 1640 medium, enriched with 10% heat-inactivated FBS, at a constant environment of 37 °C and 5% CO_2. To induce macrophage activation, the THP-1 cells were exposed to 5 ng/mL of PMA (Sigma, St. Louis, MO, USA, Cat. No. P8139) for 48 hours. For tumor-associated macrophage (TAM) activation, macrophages derived from THP-1 were treated with a conditional medium derived from tissue lysate, adjusted to a protein concentration of 50 µg/mL, for 48 hours. To induce M2 macrophages, differentiate THP-1 cells with PMA (50–100 ng/mL) (Sigma, Cat. No. P8139) for 24–48 hours, then polarize with IL-4 (10–20 ng/mL) (Sigma, Cat. No. I4269) and IL-13 (10–20 ng/mL) (Sigma, Cat. No. SRP3211) for 24–48 hours.

In vitro macrophage stimulation in Raw246.7 cells is simpler than in THP-1 cells because they are already macrophage-like and do not need a differentiation step using PMA before stimulation. Stimulus steps are the same as THP-1 cells with IL-4 and IL-13 proteins.

2.5 Tumor Infiltrating Leukocytes Extraction and Flow Cytometry

Leukocytes infiltrating tumors were isolated following previously established methods [8]. In summary, non-

Table 1. Sequence of shRNA and primers used in our research.

Category	Primers and shRNA	Sequence (5′-3′)
Human		
shRNA target oligo	*shMETTL3*	GCTGCACTTCAGACGAATT
	shCPT1A	TCCAGAGTCCGATTGATTTTTGC
Primers used in PCR	*Mettl3* forward	CTGGGCACTTGGATTTAAGGAA
	Mettl3 reverse	TGAGAGGTGGTGTAGCAACTT
	Cpt1a forward	TTCAGTTCACGGTCACTCCG
	Cpt1a reverse	TGACCACGTTCTTCGTCTGG
	Gapdh forward	CAGGAGGCATTGCTGATGAT
	Gapdh reverse	GAAGGCTGGGGCTCATTT
Mouse		
shRNA target oligo	*shMettl3*	CCTCAGTGGATCTGTTGTGAT
	shCpt1a	AGCCCTGAGACAGACTCACA
Primers used in PCR	*Mettl3* forward	CTGGGCACTTGGATTTAAGGAA
	Mettl3 reverse	TGAGAGGTGGTGTAGCAACTT
	Cpt1a forward	AGATCAATCGGACCCTAGACAC
	Cpt1a reverse	CAGCGAGTAGCGCATAGTCA
	Gapdh forward	TTGTCATGGGAGTGAACGAGA
	Gapdh reverse	CAGGCAGTTGGTGGTACAGG

essential tissue like fat, connective tissue, and necrotic material was discarded. The remaining tissue was finely chopped into pieces of 1–2 mm in RPMI 1640 (Invitrogen, CA), then transferred to conical tubes of 15 or 50 mL. These samples underwent a digestion process using a medium containing three enzymes: DNase at 30 U/mL, hyaluronidase at 0.1 mg/mL, and collagenase at 1 mg/mL (Invitrogen). This digestion occurred over 2 hours at ambient temperature with mild agitation. The tissues were then suspended in 10 mL of RPMI 1640 and strained through a 70-µm cell strainer (BD Pharmingen, San Diego, CA, USA). Any tissue retained by the strainer was individually placed into wells with 1 mL of T-cell growth medium in a 24-well plate, for further isolation or analysis via flow cytometry.

For flow cytometry and sorting, the isolated cells were first washed and then resuspended in FACS buffer (1× PBS, 2% inactivated Fetal Calf Serum (iFCS), 2 mM EDTA) for counting in a Neubauer chamber with Trypan blue (C1313S, Beyotime, Shanghai, China). Between 2 and 3 million cells were used for FACS staining. The cell suspensions were treated with a viability dye (1:400) in 1× PBS for 20 minutes. Following a wash with FACS buffer, the cells were incubated with FcR-block (1:100, C1752S, Beyotime, Shanghai, China) for 10 minutes and then sequentially stained with antibodies listed as below: CD45 (1:300, BD Pharmingen, CA, 553081), F4/80 (1:150, BioLegend, San Diego, CA, USA, 157305), CD206 (1:100, BioLegend, CA, 141719). After another wash, the samples were stained with streptavidin (A0305-0.2ml, Beyotime, Shanghai, China) for 10 minutes, fixed with 4% paraformaldehyde (PFA) (P0099-100ml, Beyotime, Shanghai, China) for 30 minutes, and then washed again with FACS buffer. The stained cells are then analyzed using a flow cytometer, where gates are set based on forward scatter (FSC) and side scatter (SSC) parameters to exclude debris and dead cells. LSRII Flow Cytometer from BD Biosciences (Franklin Lakes, NJ, USA) was utilized to assess the expression of the specific markers. The focus is on populations that are positive for CD45 and F4/80, with an emphasis on CD206 expression to identify M2 macrophages. The data was processed using FlowJo software (v10.0.7) from Tree Star Inc (Ashland, OR, USA).

2.6 An Orthotopic Mouse Model of Hepatocellular Carcinoma

Ninety 3-week-old C57BL/6 mice that consistently weigh around 13~15 g (Gemphamatec, Nanjing, China) were purchased and first subjected to a high-fat diet for eight weeks per previously successfully built animal model [13]. The Non-Alcoholic Fatty Liver Disease (NAFLD) Activity Score (NAS) for evaluating NAFLD in mouse models includes scoring steatosis (0–3), lobular inflammation (0–2), hepatocellular ballooning (0–2), and fibrosis (0–4) [14]. An orthotopic hepatocellular carcinoma (HCC) model was established using both NAFLD and non-NAFLD mice with the mouse HCC cell line Hep1-6. NAFLD mice were divided into 3 groups: Control, Group A, and Group B. To anesthetize the mice, propofol was injected into the abdomen at a dosage of 50 mg/kg. Eight weeks post-orthotopic transplantation with 3×10^6 cells. In adoptive transfer therapy using mouse macrophages, bone marrow-derived monocytes were isolated from the femurs and tibias of C57BL/6 mice and differentiated into bone

marrow-derived macrophages (BMDMs) over 7 days using complete medium (RPMI 1640 + 10% FBS) supplemented with 20 ng/mL M-CSF. Lentiviral packaging was then performed by co-transfecting HEK293T cells with either the METTL3 overexpression vector (pLVX-METTL3) or CPT1A shRNA vector along with packaging plasmids (psPAX2/pMD2.G) using Lipofectamine 3000 (Invitrogen, Carlsbad, CA, USA, Cat. No. L3000001). Viral supernatants were collected after 48 hours and concentrated. Differentiated BMDMs were pretreated with polybrene (C0351-1ml, Beyotime, Shanghai, China) (8 µg/mL) and subsequently infected with lentivirus. Finally, 5×10^6 cells were intravenously injected into tumor-bearing mice via the tail vein for therapeutic evaluation. For euthanasia, pentobarbital was injected into mice at 150 mg/kg dosage. Immediately following euthanasia, a midline laparotomy was performed, and the liver was carefully excised. For tumor volume measurement, the liver was weighed. For multiple immunohistochemistry (mIHC) staining and Hematoxylin and Eosin (H&E) staining, portions of the liver were fixed in 10% neutral buffered formalin. For other analyses (e.g., RNA and protein extraction), additional liver tissue samples were snap-frozen in liquid nitrogen and stored at –80 °C. Each group had 6 mice and every experiment was performed in triplicate.

2.7 Immunoblot and Multiple Immunohistochemistry (mIHC) Assay

Proteins were extracted from cultured cells using a Protein Extraction Kit (Kaiji, Nanjing, China). These proteins were then separated using SDS-PAGE gels and subsequently transferred onto PVDF membranes (Millipore, Burlington, MA, USA) with a pore size of 0.45 µm. For the detection process, anti-rabbit (A0208) or anti-mouse (A0216, Beyotime, Shanghai, China) horseradish peroxidase (HRP)-conjugated secondary antibodies were applied before electrochemiluminescence (ECL) detection. Multispectral images of the stained slides were captured using the Vectra 3 System (PerkinElmer, MA), ensuring consistent exposure times for each scan.

The process of mIHC staining on tissue sections was conducted using the PANO 5-plex immunohistochemistry kit (Catalog #10080100100, Panovue, Beijing, China), following the manufacturer's instructions. The procedure began with the treatment of paraffin slices in a microwave, followed by incubation with one primary antibody. These slices were then incubated with horseradish peroxidase (HRP) conjugated secondary antibodies and subjected to aminide signal amplification. The antibodies utilized included anti-METTL3 (1:50, 15073-1-AP, Proteintech, Rosemont, IL, USA), anti-CD68 (1:200, 25747-1-AP, Proteintech), anti-iNOS (1:100, 22226-1-AP, Proteintech), anti-CPT1A (1:100, 15184-1-AP, Proteintech), and anti-α-Tubulin (1:500, 80762-1-RR, Proteintech) and Biotin-conjugated Goat Anti-Rabbit IgG (H + L) (1:200, SA00004-2, Proteintech). Following the antibody staining and washes in the mIHC procedure, tissue sections were counterstained with 4′,6-diamidino-2-phenylindole (DAPI) to visualize cell nuclei. Specifically, slides were incubated with a DAPI solution at a concentration of 1 µg/mL in PBS for 5 minutes at room temperature. After incubation, slides were washed twice with PBS to remove excess DAPI. Finally, coverslips were mounted using a fluorescence mounting medium with antifade properties to preserve signal and image quality during microscopy. DAPI fluorescence was excited using a UV light source and detected in the blue emission channel. Based on full film scanning, three high-magnification fields were randomly selected from each tissue point for image capture, maintaining the same exposure time for consistency. Cell counts and fluorescence intensity were assessed using InForm Tissue Finder (version 2.0) from PerkinElmer, Waltham, MA, USA. This software also facilitated automated tissue segmentation to distinguish between tissue and blank regions.

2.8 Hematoxylin and Eosin (H&E) Staining

Liver tissues from the normal diet and high-fat diet mice were fixed, dehydrated by gradient ethanol and xylene, and then immersed in wax. The processed tissues were then sliced at 5 µm, followed by dewaxing and hydration by xylene and gradient ethanol. The slides were then stained with hematoxylin and eosin (Cat. A3429, Sigma-Aldrich, St. Louis, MO, USA).

2.9 Oil Red O Staining

Macrophages were harvested, washed twice, and fixed with 4% paraformaldehyde for 30 minutes. They were then stained with Oil Red O (Cat. Ab223796, Abcam, Cambridge, UK). After a 10-minute incubation, the cells were washed five times with double-distilled water and immediately examined under a microscope. The Oil Red O dye was extracted from the macrophages using isopropanol (563935, Sigma-Aldrich, St. Louis, MO, USA).

2.10 RNA Sequencing

Total RNA was isolated from infiltrated macrophages from the normal diet and high-fat diet using TRIzol Reagent. RNA sequencing (RNA-seq) analysis was performed at LC Biotech Inc. (Guangzhou, China).

2.11 Metabolite-Level Measurements

Metabolite analyses were performed using Gas Chromatography-Mass Spectrometry (GC-MS). For the examination of intracellular metabolites in THP-1 and THP-1-METTL3 cells, samples containing 10 million cells each were initially quenched. The metabolites were then derivatized using methoxyamine (15 mg/mL in pyridine) for 90 minutes at a temperature of 37 °C. Following this, the derivatives underwent further treatment with Bis(trimethylsilyl) trifluoroacetamide, including 1%

chlorotrimethylsilane, and 20 µL of n-hexane, for a duration of 60 minutes at 70 °C.

The metabolomics instrumental analysis was carried out using an Agilent 7890A gas chromatography system linked to an Agilent 5975 C inert Mass Selective Detector (MSD) system (Agilent Technologies, Inc., Santa Clara, CA, USA). For the separation of these derivatives, an HP-5ms fused-silica capillary column measuring 30 m in length, 0.25 mm in diameter, and with a film thickness of 0.25 µm, from Agilent J&W Scientific was utilized. Mass spectra were collected within an m/z range of 50–600, under the selected reaction monitoring mode.

To interpret the metabolic variations among the different experimental groups, Partial Least Squares-Discriminant Analysis (PLS-DA) was applied to the data of intracellular metabolites. The Variable Importance in the Projection (VIP) scoring method was employed to determine the overall impact of each variable on the PLS-DA model. Metabolites that showed significant differences were identified based on two criteria: a p-value less than 0.05 obtained from t-tests and a VIP score exceeding 1 in the PLS-DA analysis.

2.12 RNA Immunoprecipitation (RIP) Assay

The RNA Immunoprecipitation (RIP) assay was executed in line with the protocol of the RIP Kit (Geneseed Guangzhou, China). Briefly, first, cells are harvested, washed, and resuspended in a lysis buffer containing RNase inhibitors, followed by incubation on ice to facilitate lysis. The lysate is then pre-cleared with protein A beads to minimize non-specific binding before anti-mettl3 antibodies (1:50, Cat. ab195352, Abcam) are added for overnight incubation at 4 °C. After this, pre-washed beads are added to capture the antibody-antigen complexes, which are subsequently washed multiple times to remove unbound materials. After the washing phase, the complexes were eluted from the beads, followed by a purification process. The final step involved analyzing these purified complexes through RT-qPCR (TaKaRa, Dalian, China, Cat. No. RR036A). To determine the level of RNA enrichment, the quantities of precipitated RNAs were normalized against the input controls used in the experiment.

2.13 mRNA Stability Assay

Cells were initially plated in 6-well culture dishes (Cat.140685, Thermo Fisher, Waltham, MA, USA). Following seeding, they were treated with actinomycin D (Sigma, Cat. No. A9415) at a concentration of 5 µg/mL for three distinct durations: 0 hours, 3 hours, and 6 hours. This treatment was conducted as a preparatory step before RNA extraction. After extraction, the focus was on determining the stability of CPT1A mRNA by measuring its half-life. For accurate quantification, CPT1A mRNA levels were normalized to β-Actin, which served as the reference standard in this assessment.

2.14 Statistical Analysis

Statistical analyses in the study were carried out using two different software tools: R language (version 3.5.2, https://www.r-project.org/) and GraphPad Prism (version 9.0.0, GraphPad Software, Inc., San Diego, CA, USA). The embedded Kolmogorov-Smirnov (KS) test was used to test the normality of all data before comparison. For the purpose of comparing two distinct groups, a normality test was performed and followed by two-tailed Student's t-tests. In contrast, the chi-square test was applied to evaluate categorical data.

For survival analysis, the Kaplan-Meier method was employed to generate survival curves. To further assess survival data, both univariate and multivariate Cox regression analyses were conducted. Additionally, comprehensive gene analysis was performed using R language (version 3.5.2), which included Gene Ontology (GO) analysis (https://www.geneontology.org/), Kyoto Encyclopedia of Genes and Genomes (KEGG) analysis (https://www.genome.jp/kegg/), and gene set enrichment analysis (GSEA) (https://www.gsea-msigdb.org/gsea/index.jsp). In these analyses, a p-value of less than 0.05 was considered statistically significant, guiding the determination of the significance of the results obtained.

3. Results

3.1 High Fat Diet Promotes Liver Cancer Growth and Type II Differentiation of Tumor-Associated Macrophages

A high-fat diet has been implicated in the facilitation of lipid metabolism alterations and the potential advancement of hepatocellular carcinoma through metabolic reprogramming within macrophages associated with liver tumors. This hypothesis was explored using an orthotopic liver cancer model and a non-alcoholic fatty liver disease (NAFLD) model induced by a high-fat diet. Observational data indicated that a high-fat diet markedly augmented the proliferation of hepatic carcinoma. The tumor size of the normal diet mice was significantly smaller than the high-fat diet (HFD) mice, and so was the tumor weight ($p < 0.05$) (Fig. 1A,B). Concurrently, the NAFLD score was employed to assess the substantial impact of a high-fat diet on hepatic pathology. Hematoxylin and eosin (H&E) staining further substantiated the diet's facilitative role in tumor development. Morphological analysis revealed that a high-fat diet-induced NAFLD-related changes in hepatic tissue were notably characterized by an increase in vacuole-like hepatocytes. This hepatocellular vacuolation was predominantly pronounced in peritumoral regions (Fig. 1C), which is consistent with the the significant higher NAS score of HFD mice ($p < 0.001$, Fig. 1D). Subsequent extraction and flow cytometric assessment of macrophages from hepatic carcinoma tissues showed that the F4/80-CD206 double positive rate of HFD mice was significantly higher than the normal diet mice ($p < 0.001$), indicated a higher prevalence of M2

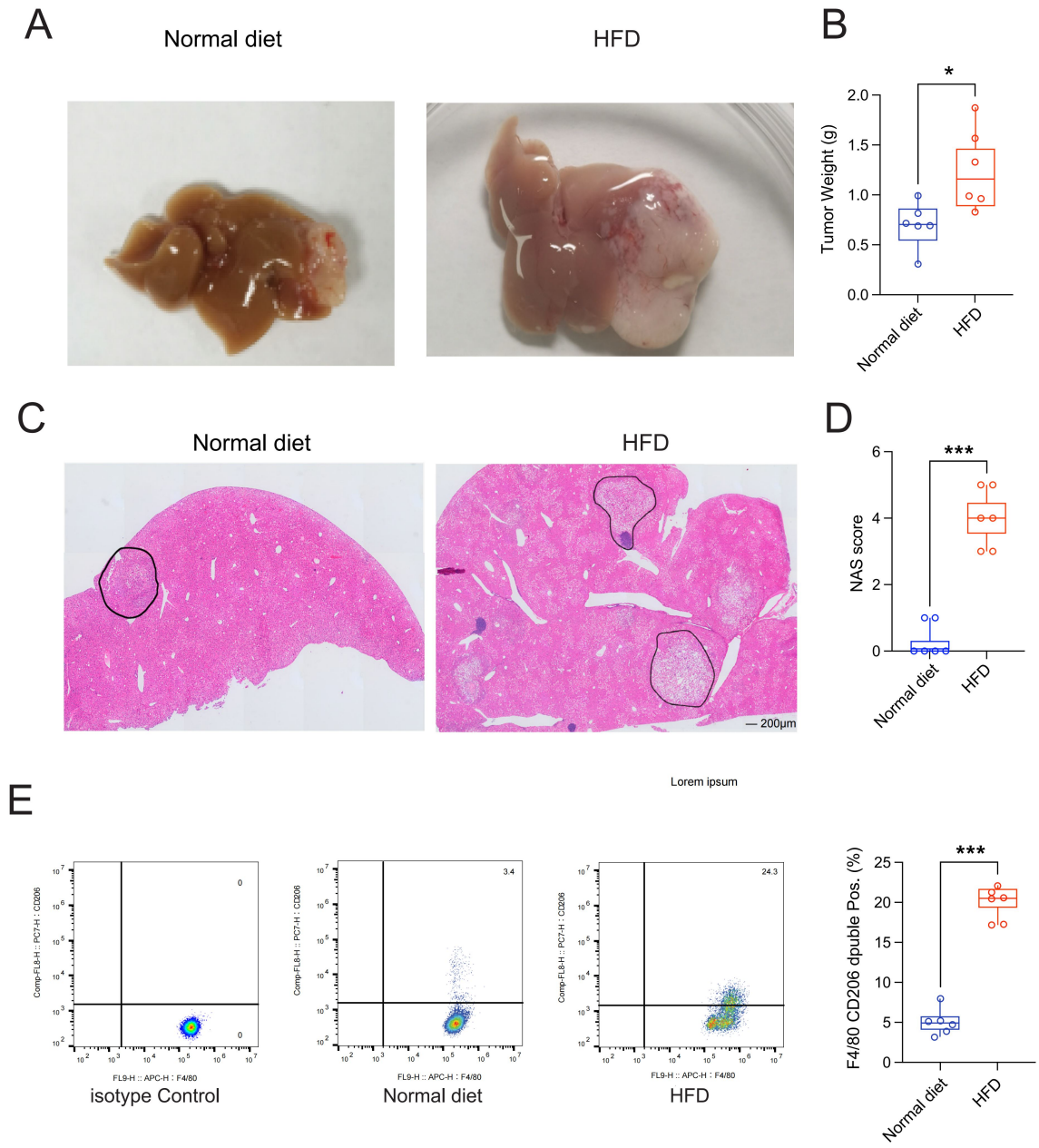

Fig. 1. Effects of high-fat diet on liver cancer growth and M2-type macrophage prevalence. (A) Construction of liver cancer models in mice through *in-situ* implantation, comparing normal diet and high-fat diet groups (n = 6). (B) Quantitative comparison of liver cancer tissue weights in both diet-based liver cancer models (n = 6). (C) Morphological analysis of *in-situ* liver cancer in mice (the area outlined by the black coil), comparing those on high-fat versus normal diets, as visualized by hematoxylin and eosin (H&E) staining (×50), Scale bar = 200 μm. (D) Assessment of Non-Alcoholic Fatty Liver Disease (NAFLD) index in the two dietary groups (n = 6). (E) Comparative analysis of M2-type macrophages in liver cancer tissues from normal and high-fat diet mice (n = 6). All experiments were performed in triplicate, and statistical significance was considered at $p < 0.05$. *$p < 0.05$; ***$p < 0.001$. HFD, high-fat diet.

macrophages within the tumor environment of NAFLD-afflicted mice (Fig. 1E).

3.2 High Fat Diet Enhances Free Fatty Acid Metabolism and RNA Modification in Hepatocellular Carcinoma Tumor-Associated Macrophages

We conducted a comparative transcriptomic analysis via RNA sequencing to delineate the transcriptional modifications in macrophages of 79 patients who adopted two dietary regimens. The analysis revealed that dietary composition precipitated marked transcriptional disparities in macrophages. Applying an adjusted *p*-value threshold of <0.05 to define statistical significance, we identified that a high-fat diet instigated the upregulation of 546 genes and the downregulation of 561 genes within hepatic carcinoma-

associated macrophages (Fig. 2A). Genes exhibiting significant upregulation encompassed *Mettl3*, *Cpt1a*, *Slc6a12*, *Eomes*, among others, whereas those demonstrating notable downregulation included *Igfbp5*, *Fcn1*, *Stc1*, among others (Fig. 2B). In contrast to the control cohort. Kyoto Encyclopedia of Genes and Genomes (KEGG) pathway enrichment analysis underscored substantial modulations in fatty acid oxidation (FAO) pathways (Fig. 2C). Concurrently, Gene Ontology (GO) enrichment analysis indicated a pronounced accumulation of gene sets associated with RNA modification as a consequence of the high-fat diet (Fig. 2D). Specifically, we observed pronounced alterations in RNA modification pathways subsequent to the administration of a high-fat diet. Through differential gene expression analysis, quantified by log-fold change (LogFC), we delineated the genes implicated in RNA methylation. We noted a marked increase in the transcriptional activity of METTL3, an enzyme responsible for N6-methyladenosine (m6A) RNA modification, suggesting its upregulation in response to lipid-rich nutritional intake (Fig. 2E). Concurrently, through comprehensive gene sequencing of FAO-related genes, it was ascertained that CPT1A, an enzyme critical to the FAO pathway, emerged as the most substantially upregulated (Fig. 2E). Additionally, the upregulation of these genes in tissue samples from the high-fat diet group was validated using Real-time PCR analysis (Fig. 2F). This observed correlation suggests a hypothesis where a high-fat diet could potentially increase the stability of *Cpt1a* mRNA ($p < 0.01$) through the upregulation of *Mettl3* ($p < 0.001$), thereby augmenting FAO metabolism within tumor-associated macrophages.

3.3 Mettl3 Gene Enhances Fatty Acid Metabolism of Macrophages by Promoting Cpt1a Gene

Subsequent to RNA sequencing (RNA-seq) analysis, we verified the co-expression pattern of *Mettl3* and *Cpt1a* in tumor-associated macrophages across diverse experimental conditions. This validation ascertained a direct proportionality in the expression levels of *Mettl3* and *Cpt1a*. Employing both human macrophage cell line THP-1 and murine macrophage cell line Raw 264.7, we engineered cellular models to either overexpress *Mettl3* or to possess knockdown constructs of *Mettl3* with concurrent *Cpt1a* suppression (**Supplementary Fig. 1**). The mRNA and protein expression of METTL3 was upregulated in *Mettl3* overexpressing cells, which were diminished by *Cpt1a* knockdown (Fig. 3A,B, $p < 0.05$). First, metabolomic profiling of THP-1 macrophages, with and without *Mettl3* overexpression, was conducted using metabolite set enrichment analysis (MSEA), Principal Component Analysis (PCA), and metabolic composition analysis. This revealed distinct metabolic reprogramming in tumor-associated macrophages, characterized by significant enrichment in fatty acid metabolism (Fig. 3C–E). To further explore the potential role of METTL3 in enhancing macrophage free fatty acid metabolism via regulation of CPT1A, we employed the aforementioned THP-1 and RAW246.7 cell models. The lipid metabolism levels in various cell populations were assessed using Oil Red O staining. Our results indicated a significant promotion of free fatty acid metabolism in macrophages mediated by METTL3. Notably, this augmentative effect was entirely abrogated following the knockdown of the *Cpt1a* gene and the percentage of oil O red cells of METTL3 OE-CPT1A shRNA is even higher than wildtype ($p < 0.001$, Fig. 3F).

3.4 Mettl3 Gene Enhances Macrophage Type II Differentiation and Its Associated Tumor Growth by Promoting Cpt1a Gene

Upon differentiation into M2 macrophages under canonical M2-polarizing conditions (interleukin-4 (IL-4) and interleukin-13 (IL-13) stimulation), we observed a pronounced augmentation in M2 phenotype specification in cells with heightened *Mettl3* expression. Conversely, cells with *Cpt1a* ablation did not exhibit a significantly different percentage of M2 macrophages than the wild type, indicating a substantial reduction in M2 differentiation propensity ($p > 0.05$, Fig. 4A). These findings implicate METTL3 in the facilitation of M2 macrophage differentiation, potentially through the stabilization or upregulation of *Cpt1a* mRNA. Beyond *in vitro* standard induction experiments, we extended our investigation to *in vivo* models to determine whether METTL3 facilitates tumor growth through the *Cpt1a* gene. Flow cytometry was used to isolate macrophages, with a successful gating strategy that identified M2 macrophages with CD206 among the F4/80 macrophage population isolated from leukocytes by applying gating based on CD45 expression (**Supplementary Fig. 2**). Macrophages were isolated from bone marrow and subjected to lentiviral-mediated gene transfection to overexpress the *Mettl3* gene in wild-type macrophages, concurrently with the knockout of the *Cpt1a* gene. Following adoptive cell therapy via tail vein injection, it was observed that macrophages overexpressing *Mettl3* significantly accelerated tumor growth ($p < 0.001$, Fig. 4B). However, this tumorigenic effect was nullified when the *Cpt1a* gene was knocked down in conjunction with *Mettl3* overexpression since the tumor weight of *Mettl3* OE-*Cpt1a* shRNA mice is not significantly different than wild type ($p > 0.05$, Fig. 4B). A similar trend was noted in the analysis of type II tumor-infiltrating macrophages, where *Mettl3* overexpression favored M2 differentiation, but this effect ceased with the *Cpt1a* knockdown, evidenced by the observation that the increase in M2 percentage of METTL3 OE-CPT1A-shRNA was not significant than control ($p > 0.05$, Fig. 4C). Consequently, our study indicates that METTL3 enhances tumor growth and type II macrophage differentiation by amplifying the effects of CPT1A in tumor-associated macrophages.

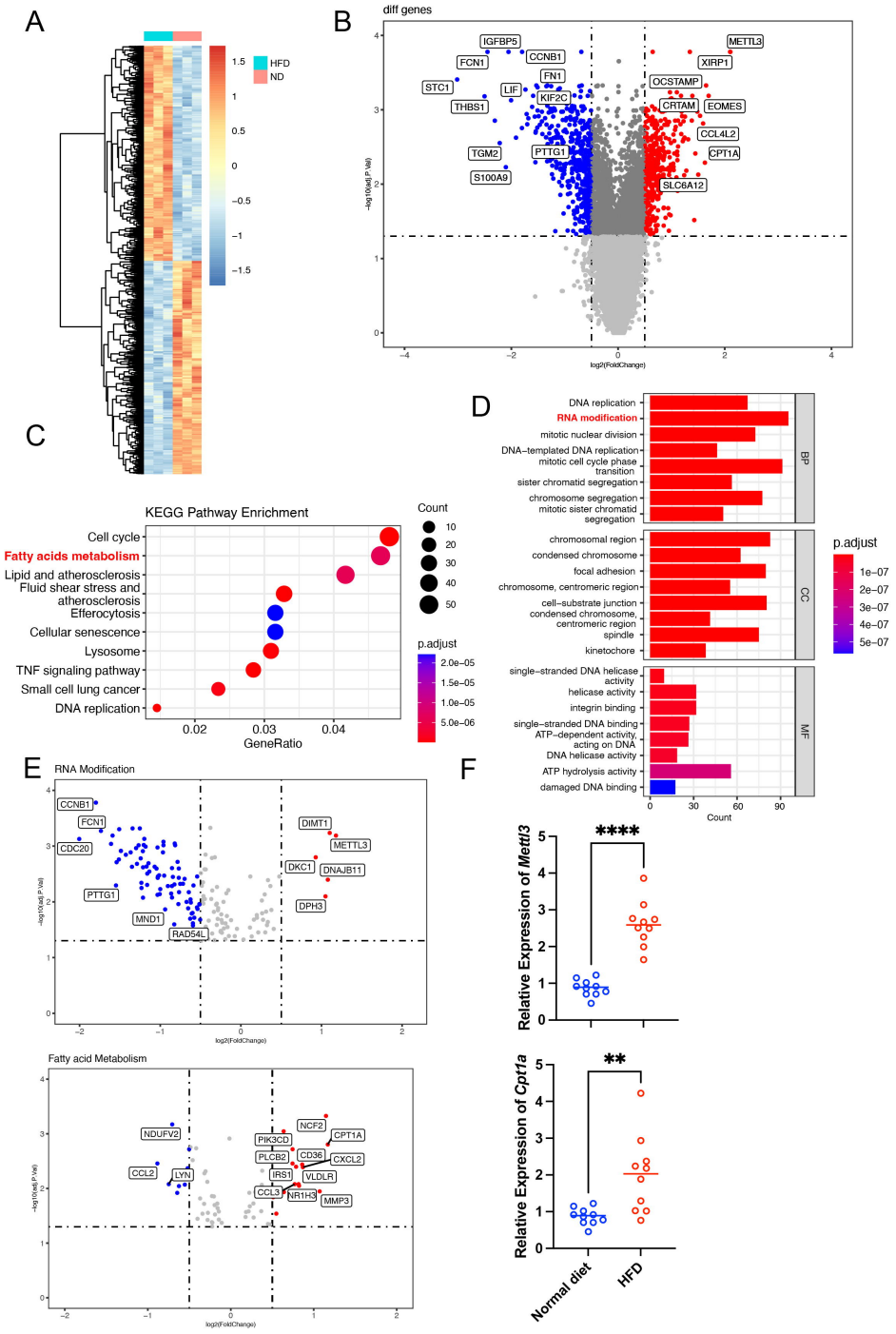

Fig. 2. Impact of high-fat diet on gene expression and metabolic pathways in liver cancer tumor-associated macrophages. (A) Heat maps illustrating the transcriptional effects on hepatoma tumor-associated macrophages under high-fat versus normal diet conditions. (B) Volcano plots highlighting the most significantly altered genes in hepatocellular carcinoma-associated macrophages, comparing high-fat and normal diets. (C) Kyoto Encyclopedia of Genes and Genomes (KEGG) pathway enrichment analysis of differentially expressed genes. (D) Gene Ontology (GO) enrichment analysis of differentially expressed genes. (E) Comparative presentation of differentially expressed genes in the "RNA Modification" and "Fatty Acid Metabolism" pathways, across the two diet groups. (F) Validation of *Mettl3* ($p < 0.001$) and *Cpt1a* ($p < 0.01$) gene expression in macrophages from liver cancer models on different diets, using real-time PCR. All experiments were performed in triplicate, and statistical significance was considered at $p < 0.05$. $^{**}p < 0.01$; $^{****}p < 0.0001$. ND, no difference.

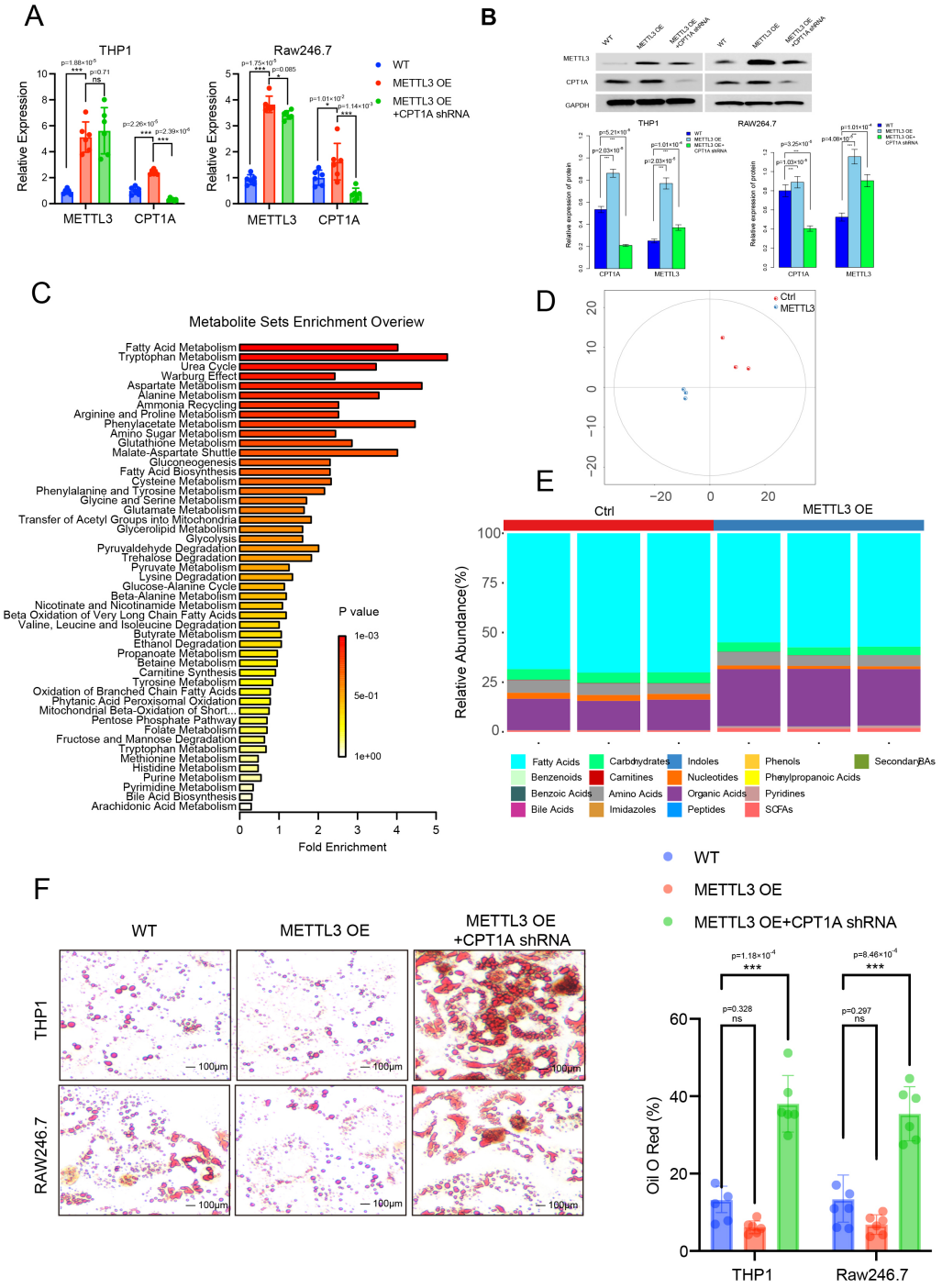

Fig. 3. Role of methyltransferase-like 3 (METTL3) in regulating fatty acid metabolism in macrophages. (A) Real-time PCR analysis for the transcription of relevant genes in various macrophage cell lines subjected to treatments as depicted (n = 6, $p < 0.05$). (B) Western blot assays to assess the protein expression levels in macrophage cell lines following the described treatments ($p < 0.05$). (C) Differential metabolite analysis using metabolite set enrichment analysis (MSEA). (D) A PCA plot illustrating the metabolomic profile of macrophages with high *Mettl3* expression. (E) Comparative analysis of METTL3's effects on macrophage metabolism, represented in a composition diagram (n = 6). (F) Oil Red O staining to visualize lipid accumulation in macrophages under different treatment conditions (n = 6). Scale bar = 100 μm. METTL3 over-expression (METTL3 OE) + CPT1A shRNA cells have drastically more lipid accumulation than wild-type control ($p < 0.001$). All experiments were performed in triplicate, and statistical significance was considered at $p < 0.05$. ns, no statistical significance; *$p < 0.05$; ***$p < 0.001$. CPT1A, carnitine palmitoyltransferase 1A.

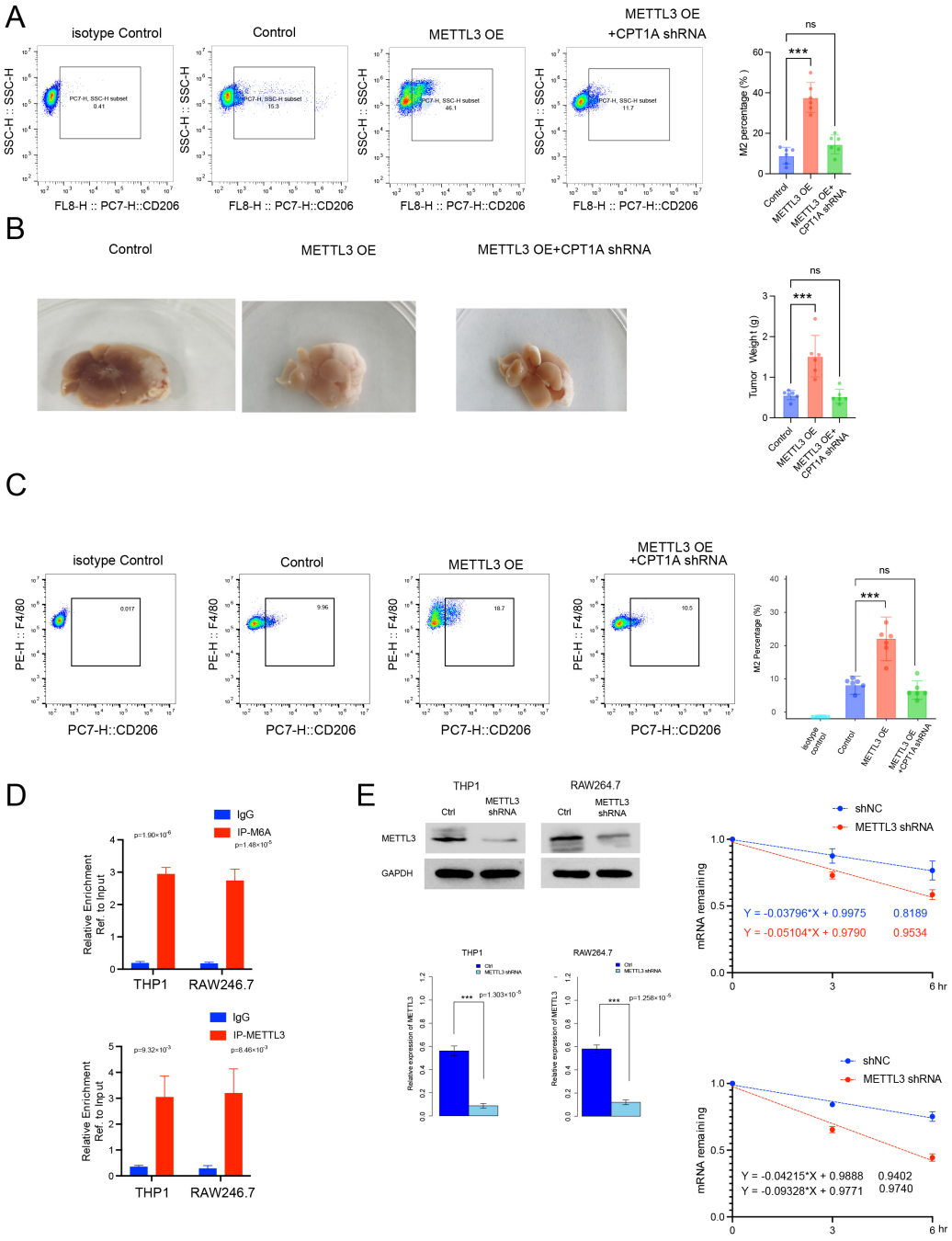

Fig. 4. Mechanism of METTL3 in enhancing macrophage fatty acid metabolism through N6-methyladenosine (m6A) modification of *Cpt1a* gene. (A) Flow cytometry analysis demonstrating the impact of various treatments on the proportion of M2-type macrophages (n = 6). (B) Investigation of the influence of different macrophage treatments on liver cancer growth, utilizing adoptive cell transfer and *in-situ* implantation models (n = 6). (C) Flow cytometry assessment of M2-type macrophage ratios in the liver cancer models described in part B (n = 6). (D) Real-time PCR analysis showing expression levels of *Mettl3* and m6A RIP-Seq enrichment of *CPT1A*/*Cpt1a* gene mRNAs (n = 6, $p < 0.001$). (E) Assessment of Igf2bp3 knockdown effects on *Cpt1a* mRNA stability in THP-1 and RAW264.7 cells. Cells were treated with 5 μg/mL actinomycin D for 0, 3, or 6 hours before RNA extraction (n = 6). All experiments were performed in triplicate, and statistical significance was considered at $p < 0.05$. ns, no statistical significance; ***$p < 0.001$. RIP-Seq, RNA immunoprecipitation sequencing.

Given the role of METTL3 as an N6-methyladenosine (m6A) methyltransferase, it was hypothesized that METTL3 may mediate m6A modifications on *Cpt1a* mRNA. To investigate this, m6A and *Mettl3* RNA immunoprecipitation sequencing (RIP-Seq) were employed to analyze macrophage transcripts. The results indicated

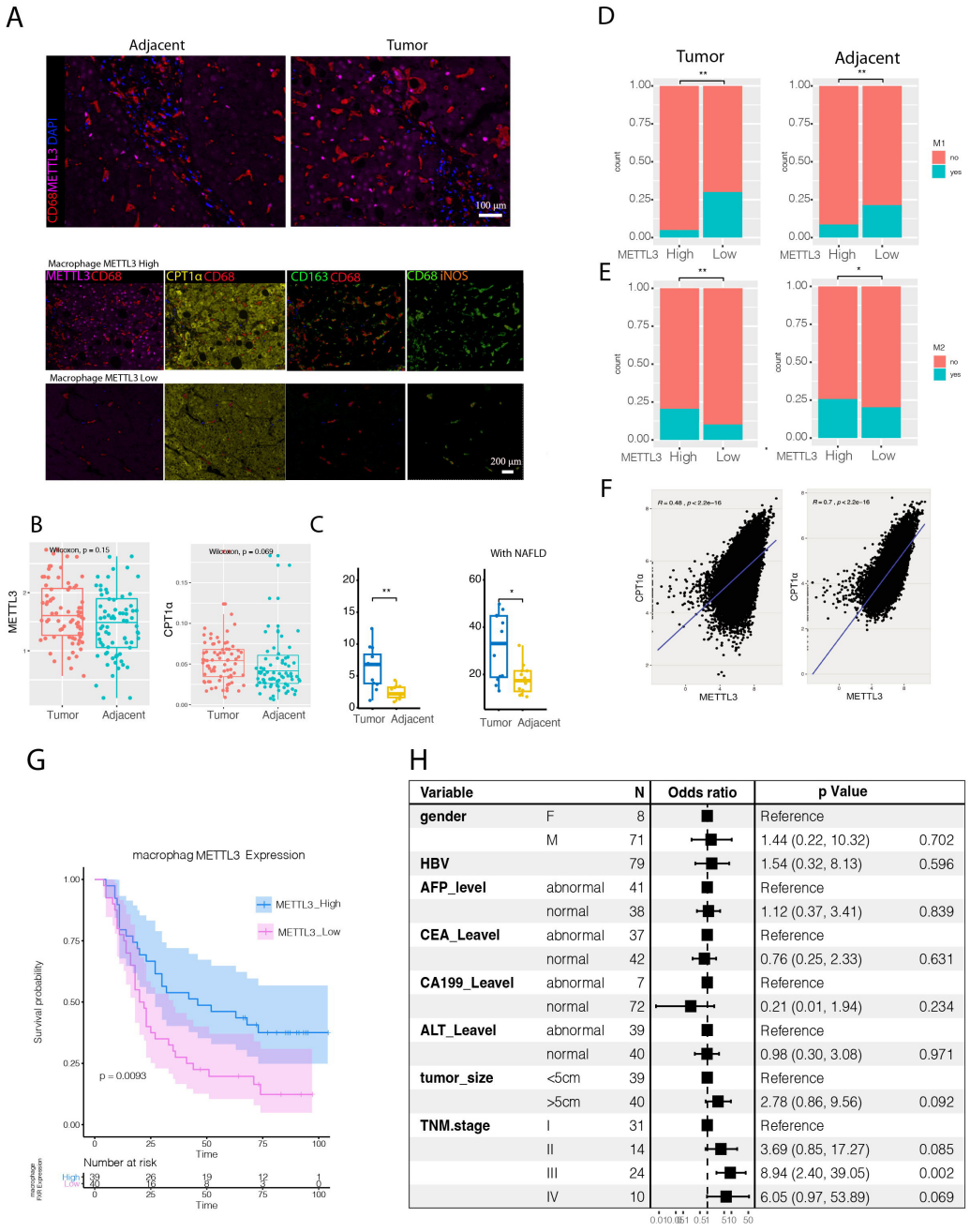

Variable		N	Odds ratio	p Value	
gender	F	8		Reference	
	M	71		1.44 (0.22, 10.32)	0.702
HBV		79		1.54 (0.32, 8.13)	0.596
AFP_level	abnormal	41		Reference	
	normal	38		1.12 (0.37, 3.41)	0.839
CEA_Leavel	abnormal	37		Reference	
	normal	42		0.76 (0.25, 2.33)	0.631
CA199_Leavel	abnormal	7		Reference	
	normal	72		0.21 (0.01, 1.94)	0.234
ALT_Leavel	abnormal	39		Reference	
	normal	40		0.98 (0.30, 3.08)	0.971
tumor_size	<5cm	39		Reference	
	>5cm	40		2.78 (0.86, 9.56)	0.092
TNM.stage	I	31		Reference	
	II	14		3.69 (0.85, 17.27)	0.085
	III	24		8.94 (2.40, 39.05)	0.002
	IV	10		6.05 (0.97, 53.89)	0.069

Fig. 5. Correlation between *Mettl3* expression in macrophages and M1/M2 ratio with prognostic implications in human hepatocellular carcinoma. (A) Multicolor immunostaining displaying the protein expression levels of CD68, iNOS, METTL3, CPT1A, and CD163 in human liver cancer (METTL3 high and low) and adjacent tissues (Scale bar = 100 μm, upper panel, Scale bar = 200 μm). (B) Comparative analysis of METTL3 and CPT1A expression in hepatoma tumor-associated macrophages within cancerous versus adjacent non-cancerous tissues. (C) Differential expression of METTL3 and CPT1A in NAFLD-associated hepatocellular carcinoma tumor-associated macrophages, contrasting cancerous with adjacent non-cancerous tissues. (D,E) Evaluation of the proportion of M1 and M2 macrophages in relation to varying levels of METTL3 expression in macrophages, compared between cancerous and adjacent non-cancerous tissues. (F) Linear correlation assessment between METTL3 and CPT1A expressions in tumor-associated macrophages in both cancerous and adjacent non-cancerous tissues. (G) Survival analysis of patients stratified by different levels of macrophage METTL3 expression. (H) Correlation analysis between macrophage METTL3 expression and clinical parameters, utilizing Cox regression. All experiments were performed in triplicate, and statistical significance was considered at $p < 0.05$. *$p < 0.05$, **$p < 0.01$. TNM, tumor node metastasis; HBV, hepatitis B virus; AFP, alpha-fetoprotein; CEA, carcinoembryonic antigen; ALT, alanine aminotransferase.

effective binding and subsequent m6A modification of *Cpt1a* mRNA by *Mettl3*. Complementary RIP assays confirmed the specificity of the CPT1A-METTL3 interaction (Fig. 4D, $p < 0.001$). Additionally, actinomycin D assays were conducted, which corroborated that METTL3 modulates the stability of *Cpt1a* mRNA across two distinct cell lines (Fig. 4E).

3.5 Correlation Between Mettl3 Expression in Macrophages and M1/M2 Ratio With Prognostic Implications in Human Hepatocellular Carcinoma

At last, we utilized a tissue array comprising 79 pairs of cancerous and adjacent non-cancerous cells to investigate m6A modifications in liver cancer-associated macrophages and their impact on macrophage fatty acids metabolism and differentiation. This was assessed using multispectral staining for CD68, iNOS, METTL3, CPT1A, and CD163 (Fig. 5A). Initially, we compared the expression levels of METTL3 and CPT1A in macrophages between tumor and adjacent tissues, finding no significant differences (Fig. 5B,C). Subsequent examination of the correlation between METTL3 expression and M1/M2 macrophage polarization revealed that macrophages expressing high levels of METTL3 exhibited a reduced M1 phenotype compared to those with low METTL3 expression. Conversely, the proportion of M2 macrophages was markedly elevated in the high METTL3 expression group relative to the low expression group, a trend consistent in both cancerous and adjacent non-cancerous tissues (Fig. 5D,E). Further studies indicated a significant positive correlation between the expression of *Mettl3* and *Cpt1a* in macrophages, both in tumor tissues and adjacent non-tumor tissues ($p < 2.2 \times 10^{-6}$, Fig. 5F). Concurrently, we observed that the death rate of patients exhibiting high macrophage expression of *Mettl3* was markedly lower compared to those with low *Mettl3* expression ($p < 0.01$, Fig. 5G). Additionally, we employed univariate Cox regression analysis after selecting significant variables by multivariate regression on the liver tissues from 79 patients. Cox regression results showed that high expression of *Mettl3* in macrophages tend to have larger tumor size and later tumor node metastasis (TNM) staging (Fig. 5H).

4. Discussion

The impact of a high-fat diet on tumor immunity is multifaceted, encompassing a range of mechanisms and outcomes. A high-fat diet may modulate immune cell functions, such as those of T cells and macrophages, altering their metabolic states and potentially affecting their efficacy and reactivity [15]. This diet could induce a pro-inflammatory tilt in immune cells, possibly enhancing anti-tumor responses or, conversely, fostering immunosuppression that benefits tumor proliferation [16]. It is also associated with heightened chronic inflammation, a condition conducive to tumor progression and dissemination. Moreover, a high-fat diet could reshape the immune cellular makeup of the tumor microenvironment, influencing, for instance, the polarization of tumor-associated macrophages, thereby facilitating tumor expansion and immune evasion [14,17]. Additionally, the expression of immune checkpoints like PD-1 and CTLA-4, crucial for T cell regulation and immune evasion, may be altered by such a diet. By activating specific metabolic pathways, including fatty acid oxidation, a high-fat diet can simultaneously influence the functions of both immune and tumor cells [15,17]. Nutritional competition within the tumor milieu, where immune and tumor cells vie for resources, can be skewed by a high-fat diet, impacting the availability and allocation of nutrients essential for immunological responses. The dichotomous nature of a high-fat diet's impact on tumor immunity—either promoting tumor growth or stimulating the immune system's tumor-fighting capabilities—varies with the diet's specifics, fat types, and consumption duration. Understanding these dynamics is vital for grasping tumor biology and advancing cancer therapeutics [18].

The intricate interplay between a high-fat diet and RNA modification in immune cells is an emerging scientific domain. Such a diet can perturb the balance of intracellular metabolites, potentially altering RNA modifications, including N6-methyladenosine (m6A), by serving as donors or cofactors [19]. This dietary pattern is known to provoke an inflammatory response, modulating the expression and activity of RNA-modifying enzymes, thereby reshaping the RNA modification landscape. In the present study, a high-fat diet significantly promotes liver cancer growth and induces type II differentiation of tumor-associated macrophages, particularly increasing M2 macrophages in NAFLD-afflicted mice. Transcriptomic analysis revealed that high-fat diet upregulates 546 genes and downregulates 561 genes in macrophages, with significant modifications in fatty acid oxidation and RNA modification pathways. Lipid-derived signaling molecules, like prostaglandins and leukotrienes, may be bolstered by a high-fat diet, influencing RNA-modifying enzymes through various signaling cascades [20]. High-fat intake can also trigger cellular stress responses, such as endoplasmic reticulum stress, which can interfere with the functions of RNA-binding proteins and modifiers [18]. Furthermore, it can impact macrophage polarization and potentially other immune cells by shifting their metabolic state, which could be linked to specific RNA modifications. These modifications, particularly m6A, are crucial in regulating differentiation and functions of T cells and B cells [21]. A high-fat diet, therefore, might indirectly modulate these pivotal immunological processes. The ramifications of such a diet on RNA modification extend to affecting immune system functionality and disease pathogenesis. Unraveling these mechanisms may illuminate the pathways through which high-fat diets influence immune regulation and disease, paving the way for novel therapeutic interven-

tions [22]. Our current research revealed that a high-fat diet induces epigenetic alterations in macrophages via the up-regulation of *Mettl3*. These modifications are advantageous in augmenting the fatty acid metabolism capabilities of macrophages.

Methyltransferase-like 3 (METTL3) serves as a pivotal epigenetic regulator within macrophages, orchestrating N6-methyladenosine (m6A) mRNA modifications, the most prevalent internal modification in mRNA [23]. These modifications are vital for mRNA stability, post-transcriptional processing, and translation efficiency. METTL3's roles in macrophages encompass Inflammatory Response Regulation: By modulating m6A modifications of inflammation-related genes, METTL3 influences macrophage activity and the subsequent inflammatory response [24]. Immune Response [25], signal Transduction and disease Progression [25,26]. In this study, we identified the up-regulation of *Mettl3* in macrophages induced by a high-fat diet. While this up-regulation might influence a spectrum of metabolism-related genes, our experimental data primarily indicate that the elevation of *Mettl3* enhances lipid metabolism in macrophages. This enhancement is achieved through the stabilization of the *Cpt1a* gene, thereby exerting an immunosuppressive effect.

Fatty acid oxidation (FAO) in macrophages is pivotal for their functionality in health and disease [26]. Essential for energy production, particularly during prolonged immune responses, FAO involves the mitochondrial breakdown of long-chain fatty acids. This process not only fuels macrophages but also influences their polarization into M1 (pro-inflammatory) and M2 (anti-inflammatory) phenotypes. M2 macrophages, which show enhanced FAO, play a key role in inflammation resolution and tissue repair [27,28]. Moreover, FAO regulates macrophage-mediated immune responses, affecting antigen presentation and cytokine secretion. In tumor environments, macrophage FAO status is crucial, with increased FAO linked to tumoricidal activity. Additionally, in metabolic disorders like obesity and diabetes, alterations in macrophage FAO can impact disease progression and inflammatory responses, underscoring FAO's comprehensive role in macrophage physiology.

Carnitine palmitoyltransferase 1A (CPT1A) is an integral enzyme in lipid metabolism, primarily facilitating the β-oxidation of long-chain fatty acids. It catalyzes their transformation into carnitine derivatives, a vital step for mitochondrial uptake and subsequent energy release through oxidative degradation [29]. Within macrophages, CPT1A drives ATP production by enhancing fatty acid beta-oxidation, meeting the high energy demands of processes like phagocytosis. It also modulates the inflammatory response by regulating fatty acid oxidation, thus influencing the production and type of inflammatory mediators and, consequently, the intensity of inflammation [30]. Additionally, variations in CPT1A activity are instrumental in macrophage polarization, shifting cells from a pro-inflammatory M1 phenotype towards an anti-inflammatory, tissue-repairing M2 state. This enzyme also indirectly modulates the immune response by affecting lipid metabolism, which can alter macrophages' antigen-presenting abilities and production of immunomodulatory factors. In the context of tumor immunity, CPT1A's role in fatty acid oxidation within the tumor microenvironment may impact macrophage-mediated tumor suppression, affecting the proliferation and survival of tumor cells. Overall, CPT1A is crucial for maintaining internal stability and combating disease by managing fatty acid β-oxidation in macrophages, thus influencing energy generation, inflammatory responses, cellular polarization, and immune regulation [31]. Clinically, high *Mettl3* expression in macrophages correlates with increased M2 phenotype, reduced patient survival, larger tumor size, and advanced TNM staging in HCC with concurrent NAFLD.

5. Conclusion

In this investigation, we developed an *in-situ* mouse liver cancer implantation model conditioned by a high-fat diet to examine its effects on macrophage gene expression. Our findings indicate that the high-fat diet induces an elevation in the m6A modification of the *Cpt1a* gene within macrophages, potentially due to increased *Mettl3* expression triggered by the diet. Although the exact mechanism by which the high-fat diet upregulates *Mettl3* remains undetermined and warrants further study, our research opens new avenues for macrophage-targeted therapies. Specifically, modulating the m6A modification level of CPT1A in macrophages could downregulate its mRNA and protein expression, thereby reversing the macrophages' metabolic profile. Such insights offer promising therapeutic strategies to counteract the metabolic reprogramming of macrophages in the context of elevated lipid levels, enhancing the efficacy of immunotherapies.

Availability of Data and Materials

The datasets used during the current study are available from the corresponding author on reasonable request.

Author Contributions

LZ was responsible for conception, design and manuscript writing. XL was responsible for collection and assembly of data. WW and XL were responsible for data analysis and interpretation. All authors were responsible for manuscript writing. All authors were responsible for the final approval of the manuscript. All authors have participated sufficiently in the work and agreed to be accountable for all aspects of the work.

Ethics Approval and Consent to Participate

This study was in accordance with the Declaration of Helsinki and approved by the Ethics in Research Committee of People's Hospital of Lianyungang (Approval No. 2021-LYG-038011). For clinical specimens, written informed consent was obtained from all participants or their families/legal guardians prior to the commencement of the study. For animal studies, all procedures involving animals were conducted in accordance with the guidelines established by Animal Welfare Act and the hospital, and approved by the ethics committee of People's Hospital of Lianyungang (Approval No.2021LYG1387).

Acknowledgment

Not applicable.

Funding

This research received no external funding.

Conflict of Interest

The authors declare no conflict of interest.

Supplementary Material

Supplementary material associated with this article can be found, in the online version, at https://doi.org/10.31083/FBL36971.

References

[1] Goldenberg RM, Gilbert JD, Manjoo P, Pedersen SD, Woo VC, Lovshin JA. Management of type 2 diabetes, obesity, or nonalcoholic steatohepatitis with high-dose GLP-1 receptor agonists and GLP-1 receptor-based co-agonists. Obesity Reviews. 2024; 25: e13663. https://doi.org/10.1111/obr.13663.

[2] Zeinabi A, Ghaedi H, Hosseini SA. Soluble Fiber Effect on Human Serum Leptin and Adiponectin: A Systematic Review and Dose-Response Meta-Analysis. Clinical Nutrition Research. 2023; 12: 320–335. https://doi.org/10.7762/cnr.2023.12.4.320.

[3] Rezler ZV, Ko E, Jin E, Ishtiaq M, Papaioannou C, Kim H, *et al*. The Impact of COVID-19 on the Cardiovascular Health of Emerging Adults Aged 18-25: Findings From a Scoping Review. CJC Pediatric and Congenital Heart Disease. 2022; 2: 33–50. https://doi.org/10.1016/j.cjcpc.2022.11.005.

[4] Firman CH, Mellor DD, Unwin D, Brown A. Does a Ketogenic Diet Have a Place Within Diabetes Clinical Practice? Review of Current Evidence and Controversies. Diabetes Therapy: Research, Treatment and Education of Diabetes and Related Disorders. 2024; 15: 77–97. https://doi.org/10.1007/s13300-023-01492-4.

[5] Antony MA, Chowdhury A, Edem D, Raj R, Nain P, Joglekar M, *et al*. Gut microbiome supplementation as therapy for metabolic syndrome. World Journal of Diabetes. 2023; 14: 1502–1513. https://doi.org/10.4239/wjd.v14.i10.1502.

[6] Brandfon S, Eylon A, Khanna D, Parmar MS. Advances in Anti-obesity Pharmacotherapy: Current Treatments, Emerging Therapies, and Challenges. Cureus. 2023; 15: e46623. https://doi.org/10.7759/cureus.46623.

[7] Brenta G, Di Fermo F. Thyroid cancer and insulin resistance. Reviews in Endocrine & Metabolic Disorders. 2024; 25: 19–34. https://doi.org/10.1007/s11154-023-09849-7.

[8] Srilatha M, Malla R, Adem MP, Foote JB, Nagaraju GP. Obesity associated pancreatic ductal adenocarcinoma: Therapeutic challenges. Seminars in Cancer Biology. 2023; 97: 12–20. https://doi.org/10.1016/j.semcancer.2023.11.002.

[9] Shi Y, Qi W. Histone Modifications in NAFLD: Mechanisms and Potential Therapy. International Journal of Molecular Sciences. 2023; 24: 14653. https://doi.org/10.3390/ijms241914653.

[10] Bołdys A, Bułdak Ł, Maligłówka M, Surma S, Okopień B. Potential Therapeutic Strategies in the Treatment of Metabolic-Associated Fatty Liver Disease. Medicina. 2023; 59: 1789. https://doi.org/10.3390/medicina59101789.

[11] Sankofi BM, Valencia-Rincón E, Sekhri M, Ponton-Almodovar AL, Bernard JJ, Wellberg EA. The impact of poor metabolic health on aggressive breast cancer: adipose tissue and tumor metabolism. Frontiers in Endocrinology. 2023; 14: 1217875. https://doi.org/10.3389/fendo.2023.1217875.

[12] Oczkowski M, Dziendzikowska K, Pasternak-Winiarska A, Włodarek D, Gromadzka-Ostrowska J. Dietary Factors and Prostate Cancer Development, Progression, and Reduction. Nutrients. 2021; 13: 496. https://doi.org/10.3390/nu13020496.

[13] Kishida N, Matsuda S, Itano O, Shinoda M, Kitago M, Yagi H, *et al*. Development of a novel mouse model of hepatocellular carcinoma with nonalcoholic steatohepatitis using a high-fat, choline-deficient diet and intraperitoneal injection of diethylnitrosamine. BMC Gastroenterology. 2016; 16: 61. https://doi.org/10.1186/s12876-016-0477-5.

[14] Arab JP, Martin-Mateos RM, Shah VH. Gut-liver axis, cirrhosis and portal hypertension: the chicken and the egg. Hepatology International. 2018; 12: 24–33. https://doi.org/10.1007/s12072-017-9798-x.

[15] Ringel AE, Drijvers JM, Baker GJ, Catozzi A, García-Cañaveras JC, Gassaway BM, *et al*. Obesity Shapes Metabolism in the Tumor Microenvironment to Suppress Anti-Tumor Immunity. Cell. 2020; 183: 1848–1866.e26. https://doi.org/10.1016/j.cell.2020.11.009.

[16] Ianiro G, Niro A, Rosa L, Valenti P, Musci G, Cutone A. To Boost or to Reset: The Role of Lactoferrin in Energy Metabolism. International Journal of Molecular Sciences. 2023; 24: 15925. https://doi.org/10.3390/ijms242115925.

[17] Bu L, Zhang Z, Chen J, Fan Y, Guo J, Su Y, *et al*. High-fat diet promotes liver tumorigenesis via palmitoylation and activation of AKT. Gut. 2024; 73: 1156–1168. https://doi.org/10.1136/gutjnl-2023-330826.

[18] Moon JS, Lee W, Cho YH, Kim Y, Kim GW. The Significance of N6-Methyladenosine RNA Methylation in Regulating the Hepatitis B Virus Life Cycle. Journal of Microbiology and Biotechnology. 2024; 34: 233–239. https://doi.org/10.4014/jmb.2309.09013.

[19] Wang MK, Gao CC, Yang YG. Emerging Roles of RNA Methylation in Development. Accounts of Chemical Research. 2023; 56: 3417–3427. https://doi.org/10.1021/acs.accounts.3c00448.

[20] Xiao L, De Jesus DF, Ju CW, Wei JB, Hu J, DiStefano-Forti A, *et al*. m6A mRNA methylation in brown fat regulates systemic insulin sensitivity via an inter-organ prostaglandin signaling axis independent of UCP1. Cell Metabolism. 2024; 36: 2207–2227.e9. https://doi.org/10.1016/j.cmet.2024.08.006.

[21] Cai Y, Yu R, Zhang Z, Li D, Yi B, Feng Z, *et al*. Mettl3/Ythdf2 regulate macrophage inflammation and ROS generation by controlling Pyk2 mRNA stability. Immunology Letters. 2023; 264: 64–73. https://doi.org/10.1016/j.imlet.2023.11.004.

[22] Losol P, Mercken LP, Fisk HL, Calder PC, Holloway JW, Torrens C. Maternal high-fat diet in mice alters immune regulation and lung function in the offspring. The British Journal of Nutrition. 2021; 126: 844–852. https://doi.org/10.1017/S0007114520004742.

[23] Brewer G. METTL3 inhibition enhances anti-tumour immunity.

Nature Reviews. Cancer. 2023; 23: 654. https://doi.org/10.1038/s41568-023-00621-2.

[24] Maldonado López AM, Ko EK, Huang S, Pacella G, Kuprasertkul N, D'souza CA, *et al*. Mettl3-catalyzed m^6A regulates histone modifier and modification expression in self-renewing somatic tissue. Science Advances. 2023; 9: eadg5234. https://doi.org/10.1126/sciadv.adg5234.

[25] Wang B, Zhang Y, Niu H, Zhao X, Chen G, Zhao Q, *et al*. METTL3-Mediated STING Upregulation and Activation in Kupffer Cells Contribute to Radiation-Induced Liver Disease via Pyroptosis. International Journal of Radiation Oncology, Biology, Physics. 2024; 119: 219–233. https://doi.org/10.1016/j.ijrobp.2023.10.041.

[26] Ren S, Xiao Y, Wang H, Zhao L, Li H, Wei L, *et al*. Abnormal genetic and epigenetic patterns of m6A regulators associated with tumor microenvironment in colorectal cancer. Translational Cancer Research. 2023; 12: 2033–2047. https://doi.org/10.21037/tcr-23-186.

[27] Xia H, Dufour CR, Medkour Y, Scholtes C, Chen Y, Guluzian C, *et al*. Hepatocyte FBXW7-dependent activity of nutrient-sensing nuclear receptors controls systemic energy homeostasis and NASH progression in male mice. Nature Communications. 2023; 14: 6982. https://doi.org/10.1038/s41467-023-42785-3.

[28] Yang T, Qu X, Wang X, Xu D, Sheng M, Lin Y, *et al*. The macrophage STING-YAP axis controls hepatic steatosis by promoting the autophagic degradation of lipid droplets. Hepatology. 2024; 80: 1169–1183. https://doi.org/10.1097/HEP.0000000000000638.

[29] Liu Z, Liu W, Wang W, Ma Y, Wang Y, Drum DL, *et al*. CPT1A-mediated fatty acid oxidation confers cancer cell resistance to immune-mediated cytolytic killing. Proceedings of the National Academy of Sciences of the United States of America. 2023; 120: e2302878120. https://doi.org/10.1073/pnas.2302878120.

[30] Xu F, Wang X, Huang Y, Zhang X, Sun W, Du Y, *et al*. Prostate cancer cell-derived exosomal IL-8 fosters immune evasion by disturbing glucolipid metabolism of $CD8^+$ T cell. Cell Reports. 2023; 42: 113424. https://doi.org/10.1016/j.celrep.2023.113424.

[31] Zheng Z, Li X, Nie K, Wang X, Liang W, Yang F, *et al*. Identification of berberine as a potential therapeutic strategy for kidney clear cell carcinoma and COVID-19 based on analysis of large-scale datasets. Frontiers in Immunology. 2023; 14: 1038651. https://doi.org/10.3389/fimmu.2023.1038651.